

## Article

# Fabrication of Hydrotalcite-like Copper Hydroxyl Salts as a Photocatalyst and Adsorbent for Hexavalent Chromium Removal

Chitiphon Chuaicham <sup>1</sup>, Karthikeyan Sekar <sup>1,2</sup>, Vellaichamy Balakumar <sup>1</sup>, Li Zhang <sup>1</sup>, Jirawat Trakulmututa <sup>3</sup>, Siwaporn Meejoo Smith <sup>3</sup> and Keiko Sasaki <sup>1,\*</sup>

- <sup>1</sup> Department of Earth Resources Engineering, Kyushu University, Fukuoka 819-0395, Japan; song@mine.kyushu-u.ac.jp (C.C.); karthik.keyan02@gmail.com (K.S.); chembalakumar@gmail.com (V.B.); zli143720@gmail.com (L.Z.)
- <sup>2</sup> Department of Chemistry, Faculty of Engineering and Technology, SRM Institute of Science and Technology, Kattankulathur 603203, India
- <sup>3</sup> Center of Sustainable Energy and Green Materials and Department of Chemistry, Faculty of Science, Mahidol University, Nakhon Pathom 73170, Thailand; jirawat.trk@student.mahidol.edu (J.T.); siwaporn.smi@mahidol.ac.th (S.M.S.)
- \* Correspondence: keikos@mine.kyushu-u.ac.jp; Tel.: +81-92-802-3338

**Abstract:** Cu-HyS-urea and Cu-HyS-NaOH, which are hydrotalcite-like copper hydroxyl salts, were prepared by two different methods, urea hydrolysis and precipitation, respectively. Both synthesis methods provided the successful formation of a copper hydroxyl salt,  $\text{Cu}_2(\text{OH})_3\text{NO}_3$ . From XRD and UV-DRS results, the product from the urea hydrolysis methods (Cu-HyS-urea) displayed higher crystallinity, small bandgap energy ( $E_g$ ), and high light absorption ability because of some intercalated carbonate anions. For the Cr(VI) removal test, the Cu-HyS-NaOH showed superior adsorption of Cr(VI) than Cu-HyS-urea due to a higher specific surface area, confirmed by BET analysis. However, the Cu-HyS-urea presented higher photocatalytic Cr(VI) reduction under light irradiation than Cu-HyS-NaOH, owing to narrow  $E_g$ , less recombination, and a high transfer of the photogenerated charge carriers, proven by the results from photoluminescence, photocurrent density, and electrochemical impedance spectroscopy. Thus, this work provides a new function of the hydrotalcite-like copper hydroxyl salts (Cu-HyS-urea and Cu-HyS-NaOH) that can be utilized not only for adsorption of Cr(VI) but also as photocatalysts for Cr(VI) reduction under light irradiation.

**Keywords:** hydrotalcite; Cr(VI) reduction; copper hydroxyl salt; photocatalyst; adsorption



**Citation:** Chuaicham, C.; Sekar, K.; Balakumar, V.; Zhang, L.; Trakulmututa, J.; Smith, S.M.; Sasaki, K. Fabrication of Hydrotalcite-like Copper Hydroxyl Salts as a Photocatalyst and Adsorbent for Hexavalent Chromium Removal. *Minerals* **2022**, *12*, 182. <https://doi.org/10.3390/min12020182>

Academic Editor: Andrey G. Kalinichev

Received: 4 January 2022

Accepted: 28 January 2022

Published: 30 January 2022

**Publisher's Note:** MDPI stays neutral with regard to jurisdictional claims in published maps and institutional affiliations.



**Copyright:** © 2022 by the authors. Licensee MDPI, Basel, Switzerland. This article is an open access article distributed under the terms and conditions of the Creative Commons Attribution (CC BY) license (<https://creativecommons.org/licenses/by/4.0/>).

## 1. Introduction

The hydrotalcite-like hydroxy salt (HyS) materials have been reported in one type of layered metal hydroxides, with the general formula  $\text{M}^{2+}(\text{OH})_{2-x}(\text{A}^{m-})_{x/m} \cdot n\text{H}_2\text{O}$ , where  $\text{M}^{2+}$  is the divalent metal cation ( $\text{Mg}^{2+}$ ,  $\text{Ni}^{2+}$ ,  $\text{Zn}^{2+}$ ,  $\text{Ca}^{2+}$ ,  $\text{Cd}^{2+}$ ,  $\text{Co}^{2+}$ , and  $\text{Cu}^{2+}$ ) and  $\text{A}^{m-}$  is the counterion, such as nitrate and carbonate anions, which are exchangeable anions [1]. Recently, HyS has been a promising material for various applications, including adsorption, catalytic wet oxidation, and catalytic wet peroxide oxidation. Among them, copper hydroxy salt ( $\text{Cu}_2(\text{OH})_3\text{NO}_3$ , Cu-HyS) has been focused to be an environmentally friendly material to remove toxic pollutants in wastewater [2–9]. The Cu-HyS structure belongs to the P21 space group with  $z = 2$ ; the crystal system is monoclinic with  $\beta = 94.619^\circ$  and cell characteristics of  $a = 5.6005 \text{ \AA}$ ,  $b = 6.0797 \text{ \AA}$ , and  $c = 6.9317 \text{ \AA}$  at  $25^\circ\text{C}$ . Cu octahedral layers are stacked upon each other to form the lamellar structure, containing two forms of copper octahedral: Cu(1) is coordinated by four  $\text{OH}^-$  groups and two oxygen atoms belonging to  $\text{NO}_3^-$  groups. For another Cu(2) species, four hydroxyls coordinate the Cu(2) atoms, with the fifth OH standing a little further away and an oxygen atom belonging to the  $\text{NO}_3^-$  groups. Cu octahedra create stoichiometry layers as  $[\text{Cu}_2(\text{OH})_3]^+$ . In between the

Cu octahedral layers,  $\text{NO}_3^-$  ions balance the charge between the positive layers and are bonded [10].

Cu-HyS is a key component for several applications. Because of its potential applications as a catalyst, ion exchanger, adsorbent, and precursor of copper compounds such as CuO,  $\text{Cu}_2\text{O}$ , and  $\text{Cu}(\text{OH})_2$ , it has sparked a lot of attention [8]. Moreover, Cu-HyS nanoparticles with diverse morphologies have been prepared using a variety of synthetic approaches. Liu et al. used a solvothermal approach to make single-crystalline virtually monodispersed Cu-HyS nanorods and nanobelts in 2-propanol [11]. Cu-HyS nanoribbons were explored by Yu et al. by gently hydrolyzing Cu-HyS aqueous solution in the presence of ethanolamine at low temperatures [12]. Cu-HyS nanosheets were prepared by Wang et al. using a sonochemical technique [6].

For wastewater remediation application, ultra-fast catalytic wet oxidation of methyl orange using a  $\text{Cu}_2(\text{OH})_3\text{NO}_3/\text{ZnO}$  composite was reported by Sriksaow et al. [13]. Moreover, in the same research group, remediation of phenol via catalytic wet peroxide oxidation using Zn-containing Cu hydroxide nitrate was reported [3]. For catalytic conversion application,  $\text{Cu}_2(\text{OH})_3\text{NO}_3$  was applied for the valorization of vanillic alcohol via oxidation [2]. Moreover, Cu-HyS-decorated fumed silica hybrid composites were prepared and utilized as antibacterial agents [14]. Wang et al. reported that  $\text{Cu}_2\text{O}/\text{Cu}_2(\text{OH})_3\text{NO}_3$  composites showed the excellent adsorption and degradation of methyl orange when  $\text{Cu}_2\text{O}$  acts as a main catalyst and  $\text{Cu}_2(\text{OH})_3\text{NO}_3$  is a supporting material [5]. However, the photocatalytic activity of Cu-HyS has never been reported and studied. Photocatalysis is a unique approach that is widely used and utilized in a variety of interdisciplinary study areas, including the degradation of a variety of inorganic/organic hazardous pollutants in wastewater, air purification, insecticides, and so on [15–20].

Therefore, the present work consists of synthesizing hydrotalcite-like Cu-HyS by two different methods, which were urea hydrolysis and precipitation. Their as-prepared samples were applied for photocatalysis, which is a remarkable and popular process for the oxidation and reduction of organic and inorganic pollutants in wastewater [21–23]. Additionally, the physical and chemical properties of the synthesized samples were investigated by several techniques, as shown experimentally. Moreover, the separation and transfer mechanism of the electron–hole pairs in the composite were further elucidated and proposed. Furthermore, Cu-HyS was applied for elucidating the photocatalytic reduction of hexavalent chromium (Cr(VI)), which is a toxic inorganic pollutant in wastewater [19,24–28], under light irradiation. Remarkably, Cr(VI) was placed third among the most common harmful environmental contaminants found in wastewater from various industries such as leather tanning, pigment production, and medicine, among others. The Cr(VI) concentration level in safe drinking water should be less than 0.05 mg/L, according to the World Health Organization. Cr(VI) not only has a high water solubility and a powerful carcinogenic effect, but it can also quickly permeate the body through digestion, the respiratory tract, and the skin, causing significant harm to most living species. The free discharge of Cr(VI) effluent has had a significant impact on human health and quality of life in recent years [29]. Recently, there are several methods to remove or decrease the toxicity of Cr(VI) such as the electro-Fenton process, adsorption, photocatalysis, and electrocoagulation [30–35]. Thus, the findings in this work could elucidate the advantages of using Cu-HyS in diverse applications, which are not only for the removal of organic/inorganic pollutants in wastewater by adsorption or catalytic wet oxidation process, but also it can act as photocatalyst, which can improve the removal efficiency for wastewater treatment.

## 2. Materials and Methods

### 2.1. Chemicals

Copper nitrate trihydrate ( $\text{Cu}(\text{NO}_3)_2 \cdot 3\text{H}_2\text{O}$ , purity = 99.9%), urea ( $\text{CH}_4\text{N}_2\text{O}$ , purity = 99.0%), sodium hydroxide (NaOH, purity  $\geq 97.0\%$ ), and ethanol ( $\text{C}_2\text{H}_5\text{OH}$ , purity  $\geq 97.0\%$ ) were received from Wako Chemicals, Osaka, Japan. 5,5-Dimethyl-1-pyrroline N-Oxide (DMPO,

purity  $\geq 97.0\%$ ) was purchased from TCI, Japan. Potassium dichromate ( $K_2Cr_2O_7$ ,  $\geq 99.0\%$ ) was purchased from Sigma-Aldrich.

### 2.2. Synthesis of Hydrotalcite-like Copper Hydroxyl Salts

Hydrotalcite-like copper hydroxyl salts were prepared by two different methods, which were urea hydrolysis and precipitation. For the urea hydrolysis, 6.0 g of urea was added into 50 mL of 1.0 mM  $Cu(NO_3)_2 \cdot 3H_2O$  aqueous solution under stirring at room temperature for 30 min. After that, the above solution was transferred to a Teflon-lined stainless-steel autoclave for hydrothermal treatment at 100 °C for 120 min. The solid product was separated, washed with de-ionized water, and dried at 75 °C for 24 h. The obtained product from urea hydrolysis was denoted as Cu-HyS-urea. For the precipitation method, 10 mL of 0.01 mM NaOH solution was dropped into 50 mL of 1.0 mM  $Cu(NO_3)_2 \cdot 3H_2O$  solution under stirring at room temperature for 120 min. The solid product was collected by filtration, washed with de-ionized water, and dried at 75 °C for 24 h. The yielded product from the precipitation method was denoted as Cu-HyS-NaOH.

### 2.3. Characterization

The crystal phase structures of Cu-HyS-urea and Cu-HyS-NaOH were detected by utilizing an Ultima IV X-ray diffraction (XRD) instrument (RIGAKU, Akishima, Japan), using Cu  $K\alpha$  radiation with 40 kV acceleration voltage and 40 mA applied current at a 2°/min scanning speed and 0.02° step size. The chemical properties and functional groups of Cu-HyS-urea and Cu-HyS-NaOH were determined using Fourier transform infrared (FTIR) spectroscopy using a JASCO FTIR-670 Plus (Tokyo, Japan), resolution at 4  $cm^{-1}$ , scan time = 16 in transmission mode. The FTIR samples were prepared by KBr method. The obtained FTIR results were processed using the ejsw2000 program for baseline correction. The morphology, surface properties, and dispersion of all elements of Cu-HyS-urea and Cu-HyS-NaOH were confirmed by scanning electron microscope (SEM-EDX) (Hitachi, Tokyo, Japan: FlexSEM 1000II and AZteclive lite FX). For the EDX results, we processed the EDX results including baseline correction using the Aztec program from AZteclive lite FX). The light absorption ability of the Cu-HyS-urea and Cu-HyS-NaOH was determined by UV-DRS (UV-2450 Shimadzu, Kyoto, Japan) equipped with an ISR-2200 integrating sphere attachment (Kyoto, Japan). In this experiment, we used  $BaSO_4$  as a baseline, which has no light absorption in the measurement region. The valence band positions of Cu-HyS-urea and Cu-HyS-NaOH were measured by X-ray photoelectron spectroscopy (XPS) (ESCA 5800; ULVAC-PHI, Inc., Kanagawa, Japan) using a monochromated Al  $K\alpha$  X-ray source at 200 W. The data analysis was conducted using Casa XPS software (version 2.3.12.8). Binding energy was calibrated using  $E_B[C\ 1s] = 284.6$  eV, which was assigned to the contamination peak derived from vacuum oil in the apparatus. Photoluminescence spectroscopy (PL) was performed by an FP-6600 spectrofluorometer (FP-6600 spectrofluorometer, JASCO Corporation, Tokyo, Japan) with excitation wavelength at 330 nm, emission wavelength ranges of 400–480 nm with the maximum emission peak at 442 nm. Electrochemical impedance spectroscopy (EIS) measurements were conducted using 1280c AMETEK advanced measurement technology, Berkshire, United Kingdom. For the electron spin resonance (ESR) experiment, the reactive species determinations were explored at room temperature by suspending the catalyst in water or methanol at the same amount of loading as the photocatalytic activity under light irradiation. Before measurement, 50 mM of 5,5-Dimethyl-1-pyrroline N-oxide (DMPO), used as the radical trapping reagent, was added into the reaction mixture. ESR signal at X-band frequency (9.846 GHz) was obtained by Bruker ELEXSYS (ER083CS) spectroscopy, which the operating parameters of were set as microwave power = 20 mW, modulation amplitude = 1 G, modulation frequency = 100 kHz, and modulation amplitude = 1 G. The interpretation of radical species was analyzed by WinSim2002 program.

#### 2.4. Photocatalytic Test

The photocatalytic performance of the Cu-HyS-urea and Cu-HyS-NaOH was estimated by conversion of Cr(VI) under light illumination (500 W Xe lamp, Ushio Inc., Tokyo, Japan) that provided UV–visible light irradiation (Figure S1). For the reaction procedure, 50 mg of the sample was suspended in 50 mL of 10 ppm Cr(VI),  $K_2Cr_2O_7$ , at pH = 6 and 1 mL of ethanol as hole scavenger to avoid the re-oxidation of Cr(III) from the photocatalytic reaction in the dark for 30 min to achieve adsorption–desorption equilibrium. Then, the suspended solution was stirred under light irradiation with the temperature controlled at 25 °C. During the light illumination, the suspension was withdrawn at intervals with a syringe and filtrated through a 0.45  $\mu$ m membrane filter to remove the solid samples. The remaining concentration of Cr(VI) in the filtrated solution was evaluated by UV–Vis spectrophotometer at 260 nm. Moreover, in the cyclic reusability experiment, we directly used the spent catalyst without any treatment.

### 3. Results

#### 3.1. Characterizations

The crystal phase structure of pure Cu-HyS-urea and Cu-HyS-NaOH was investigated using the XRD technique, and their results are shown in Figure 1a. The Cu-HyS-urea and Cu-HyS-NaOH show main diffraction peaks at  $2\theta$  around 12.8° and 25.8°, which correspond to the (001) and (002) planes of the crystal phase of copper hydroxide nitrate,  $Cu_2(OH)_3NO_3$  (CSD: 250341 (ICSD) [36,37]. However, the (001) plane of Cu-HyS-urea shows a slight shift to a higher diffraction angle, compared with Cu-HyS-NaOH, suggesting some intercalation of  $CO_3$  in the structure of the  $Cu_2(OH)_3NO_3$  structure due to the decomposition of urea in the urea hydrolysis method (Figure 1b). Compared with nitrate intercalation, the higher charge density of the carbonate reduced the basal spacing to a lower value, resulting in the shifting of the (001) plane to a higher diffraction angle [38].

Moreover, the intercalation of a chemical agent into a structure usually involves its expansion and subsequent shift to the lower  $2\theta$  region. Furthermore, the observed peaks at  $2\theta = 21.6^\circ, 29.7^\circ, 32.2^\circ, 33.7^\circ, 36.6^\circ, 39.8^\circ, 41.9^\circ, 43.6^\circ, 53.1^\circ, 58.44^\circ, 60.8^\circ, \text{ and } 62.65^\circ$  can be assigned to the (110), (012), (021), (201), (121), (202), (122), (122), (123), (223), (204), and (322) planes of/belonging to  $Cu_2(OH)_3NO_3$  (Figure 1c). Thus, these XRD diffraction peaks of the product from the two different methods, urea hydrolysis and precipitation, confirmed the successful formation of  $Cu_2(OH)_3NO_3$ . Moreover, it has no characteristic diffraction peaks of impurity such as remaining urea, NaOH, and copper oxide, implying that their obtained products have only one crystalline phase of  $Cu_2(OH)_3NO_3$ . In comparison, the Cu-HyS-urea showed higher peak intensity than the Cu-HyS-NaOH because the hydrothermal step in the urea hydrolysis method can improve the crystallinity of the  $Cu_2(OH)_3NO_3$  phase of the Cu-HyS-urea.

Moreover, the chemical properties of Cu-HyS-urea and Cu-HyS-NaOH were investigated using FTIR, as presented in Figure 1d. Cu-HyS-NaOH and Cu-HyS-urea show a strong signal in the low-wavenumber region at approximately 507, 672, and 883  $cm^{-1}$ , which can be ascribed to the Cu–O–H in the structure of  $Cu_2(OH)_3NO_3$  [10]. The stretching modes of OH- groups contained in the layered structure and water molecules were attributed to the strong bands centered at  $\sim 3600\text{ cm}^{-1}$  and  $\sim 3440\text{ cm}^{-1}$ , respectively [39]. The peaks of  $NO_3^-$  groups at 785, 1044, and 1423  $cm^{-1}$  can be observed in both samples [10,40]. Moreover, the stronger additional broad vibrational peaks at 1338  $cm^{-1}$  from the carbonate anion were found in Cu-HyS-urea compared with Cu-HyS-NaOH due to a by-product from the urea hydrolysis method [41]. Thus, the intercalated anion of Cu-HyS-urea should be a carbonate and nitrate anion, whereas the intercalated anion of Cu-HyS-NaOH was only a nitrate anion.

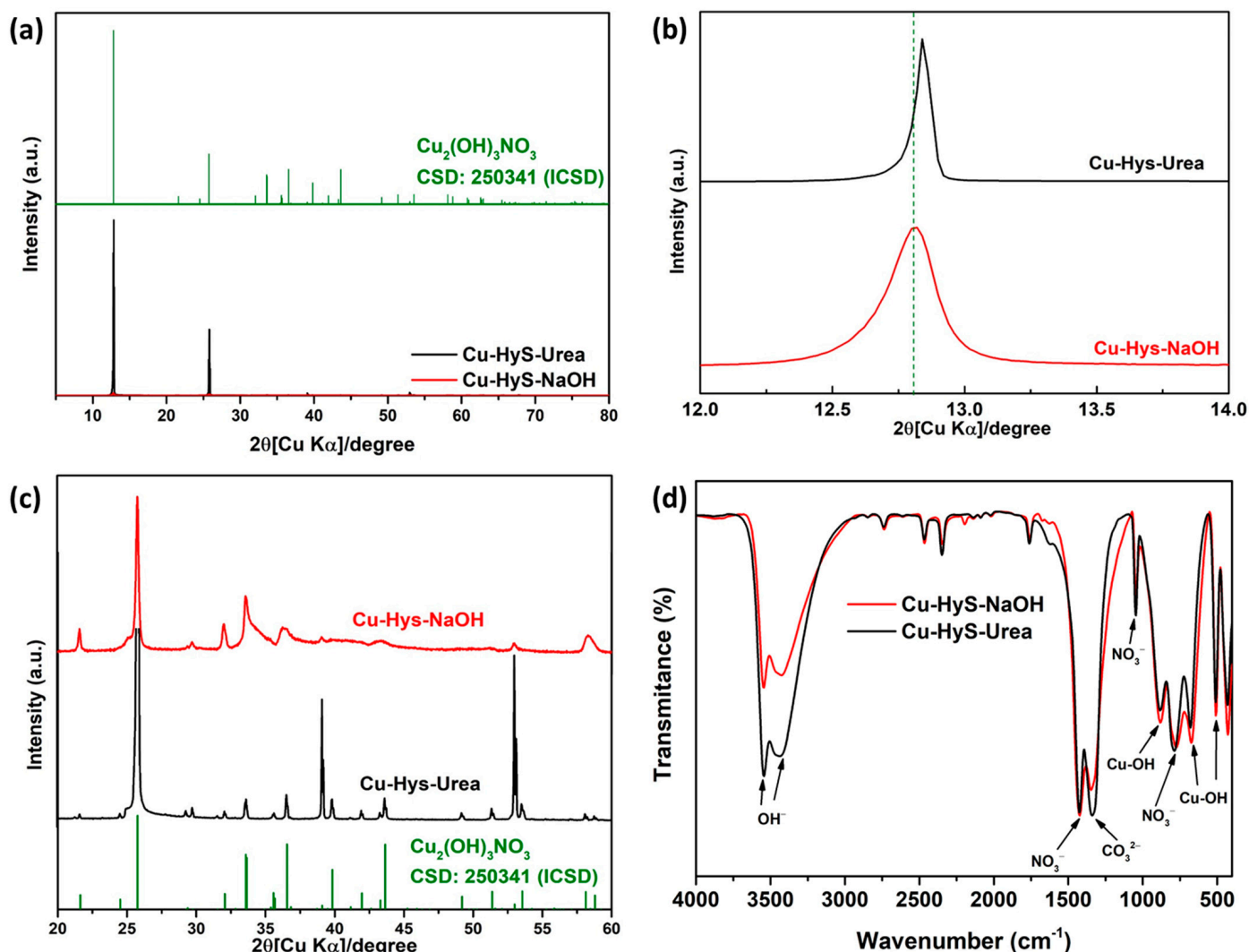


**Figure 1.** XRD patterns (a) at measurement range from  $2\theta = 5^\circ$ – $80^\circ$ , (b) at measurement range from  $2\theta = 12^\circ$ – $14^\circ$ , (c) at measurement range from  $2\theta = 20^\circ$ – $60^\circ$ , and (d) FTIR spectra of Cu-HyS-urea and Cu-HyS-NaOH.

The optical properties such as adsorption of light and energy bandgap ( $E_g$ ) of Cu-HyS-urea and Cu-HyS-NaOH, which influence photocatalytic activity, were determined by UV-DRS investigation. In Figure 2a, Cu-HyS-urea showed a main light absorption edge around 400–450 nm, which confirms the Cu-HyS-urea can be utilized as photocatalyst under the visible light region, while Cu-HyS-NaOH exhibits an absorption edge around 350–400 nm, confirming that it can adsorb light under the UV light region. The difference of intercalated anions between the layers of copper hydroxyl salt may affect the light-harvesting properties of the as-prepared products. In comparison, the Cu-HyS-urea showed a stronger light absorption ability in the visible light and near UV light regions than Cu-HyS-NaOH. This result suggested that the presence of the carbonate anion in the Cu-HyS-urea can enhance the light-harvesting ability of photocatalysts, leading to enhanced photocatalytic activity due to the substantial generation of photogenerated charge carriers participating in photocatalysis. The  $E_g$  is estimated by extrapolating the linear portion of the plot of  $(\alpha h\nu)^{1/2}$  versus  $h\nu$  to  $y$ -axis = 0 to obtain the  $E_g$  value. In Figure 2b, the  $E_g$  values of Cu-HyS-urea and Cu-HyS-NaOH were calculated to be 2.95 eV and 3.39 eV, respectively. The  $E_g$  is in good agreement with the adsorption edge of Cu-HyS-NaOH around 360 nm and Cu-HyS-urea around 420 nm. The decrease of  $E_g$  values of Cu-HyS-urea might improve the

electron–hole pair separation, which enhanced photocatalytic performance under visible light irradiation.

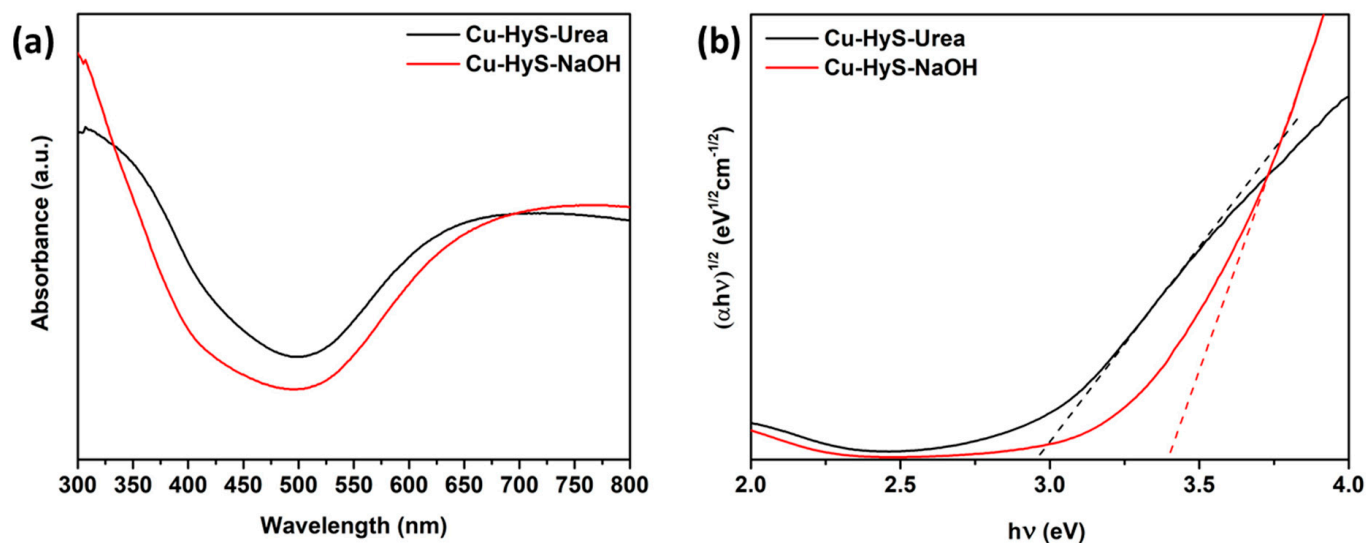


**Figure 2.** (a) DRS-UV spectra and (b) Tauc plot of Cu-HyS-urea and Cu-HyS-NaOH.

The surface structure morphology and distribution of each element in the Cu-HyS-urea and Cu-HyS-NaOH by SEM-EDX are shown in Figure 3. From Figure 3a,b, the Cu-HyS-urea displayed a large particle and high crystallinity of sheet-like structure, while the Cu-HyS-NaOH presented the low crystallinity of small plate-like particles. Moreover, both samples showed a good distribution of Cu and O, which are the main elements in the  $\text{Cu}_2(\text{OH})_3\text{NO}_3$ . The SEM results supported that the two different methods, urea hydrolysis and precipitation, provided the successful formation of  $\text{Cu}_2(\text{OH})_3\text{NO}_3$  with the different surface structure and morphology. Furthermore, the Cu content in the Cu-HyS-urea and Cu-HyS-NaOH was investigated using EDX results, as shown in Figure 3c,d. The Cu-HyS-urea showed Cu content around 79% wt, while the Cu-HyS-NaOH presented around 61% wt of Cu content, indicating that the urea hydrolysis method can provide a higher Cu-rich  $\text{Cu}_2(\text{OH})_3\text{NO}_3$  than Cu-HyS-NaOH, which might improve the photocatalytic activity. A higher Cu content of Cu-HyS-urea than Cu-HyS-NaOH may be the reason for the high crystallinity and perfect crystal (less defect of Cu) of  $\text{Cu}_2(\text{OH})_3\text{NO}_3$ , confirmed by XRD and SEM results.

The nitrogen sorption isotherm plot of both samples as presented in Figure 4a shows a type IV isotherm nature with a narrow H3-type of the hysteresis loop, suggesting that the Cu-HyS-urea and Cu-HyS-NaOH have pore channels similar to a clay mineral. Moreover, the specific surface area (SSA) of both samples was calculated using BET analysis. It can be seen that the high crystallinity of the Cu-HyS-urea sample showed smaller SSA around  $0.34 \text{ m}^2/\text{g}$  than the Cu-HyS-NaOH sample ( $14.07 \text{ m}^2/\text{g}$ ). Thus, the higher SSA of the Cu-HyS-NaOH can provide a more active surface to adsorb the target Cr(VI) anion in the reaction.

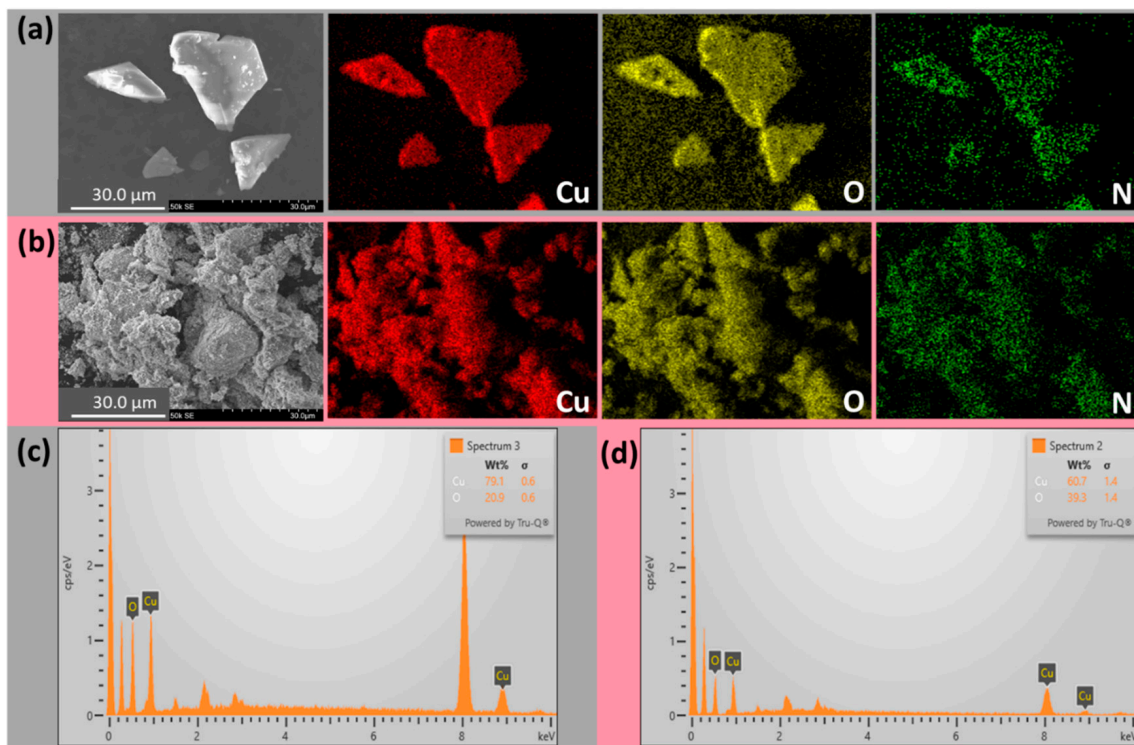


Figure 3. SEM of (a) Cu-HyS-urea and (b) Cu-HyS-NaOH, and EDX of (c) Cu-HyS-urea and (d) Cu-HyS-NaOH.

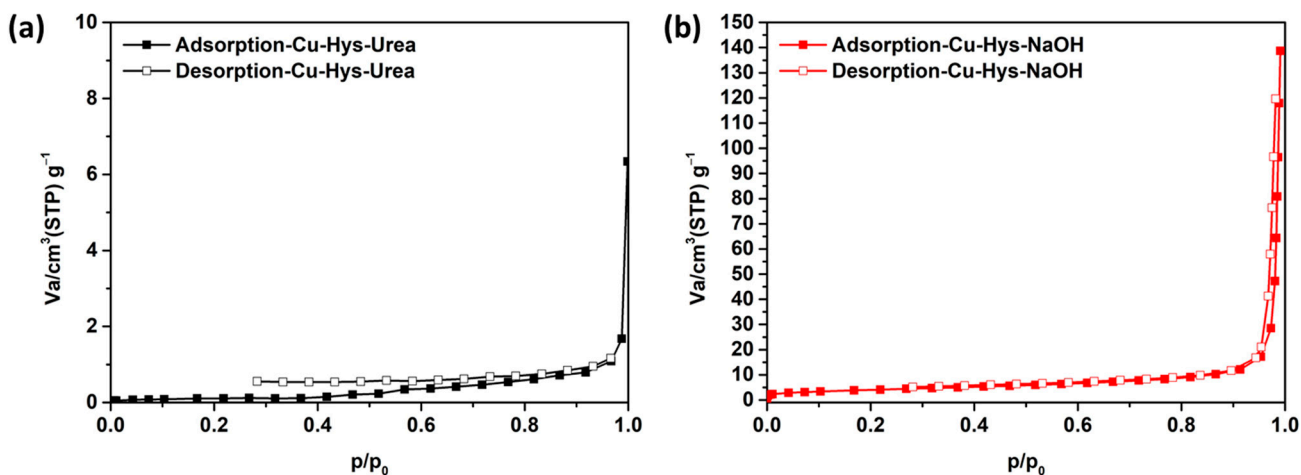
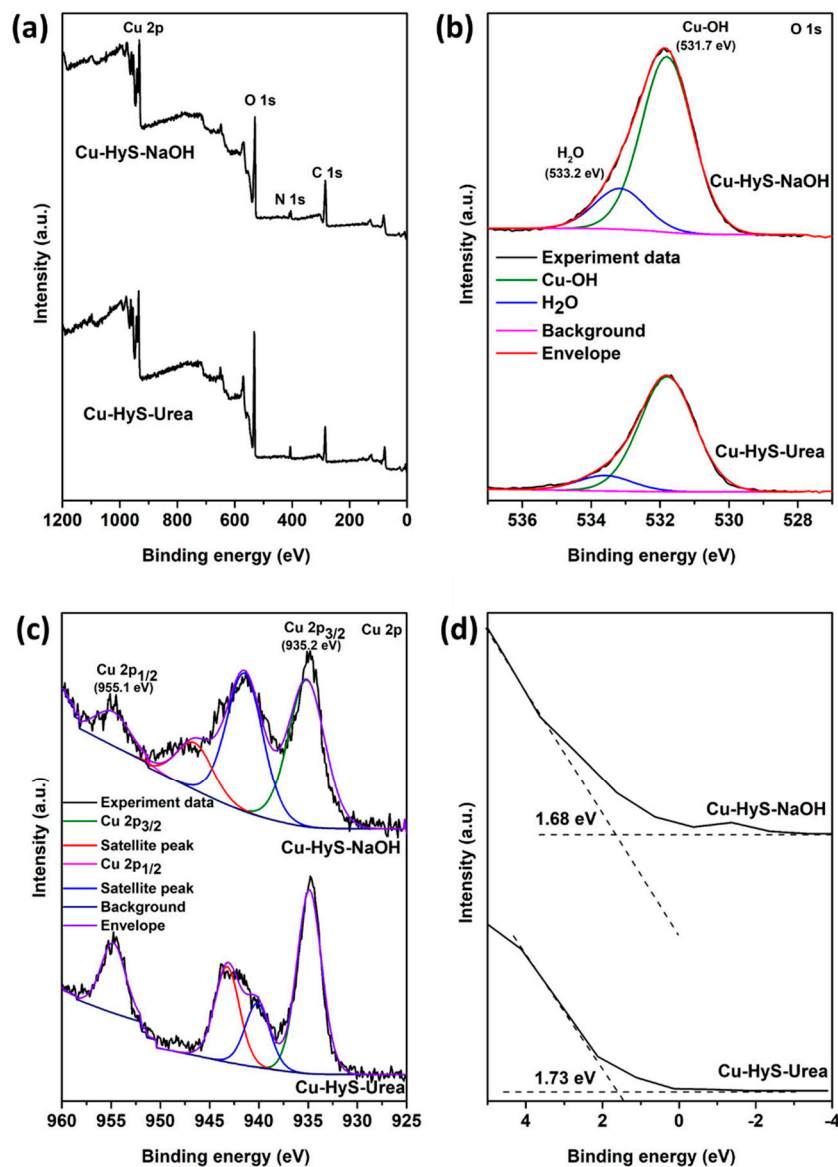


Figure 4. Nitrogen adsorption–desorption isotherm of (a) Cu-HyS-urea and (b) Cu-HyS-NaOH.

The chemical state and species, including valence band (VB) positions of Cu-HyS-urea and Cu-HyS-NaOH, were determined using XPS analysis, as shown in Figure 5a. The survey scans of the Cu-HyS-urea and Cu-HyS-NaOH show the clear observation peaks of the Cu and O atoms, which are the main elemental components in the  $\text{Cu}_2(\text{OH})_3\text{NO}_3$ . To elucidate the oxidation state and species of Cu, the narrow scan in the Cu 2p orbital region was observed, as shown in Figure 5b. The main peaks at 935.2 eV of the Cu 2p<sub>3/2</sub> orbital of the Cu-HyS-urea and Cu-HyS-NaOH can be assigned to divalent Cu in hydroxide form, while the satellite peaks of Cu atoms can be observed around 940–947 eV for both samples [42]. In Figure 5c of O 1s orbitals, the O 1s spectra of both samples can be deconvoluted into two components, which are Cu–OH bond and molecular water for the peak at approximately 532.3 and 534.1 eV, respectively [43]. Furthermore, the valence band (VB) of the Cu-HyS-urea and Cu-HyS-NaOH was determined by XPS analysis, as

shown in Figure 5d. The estimated VB of Cu-HyS-urea and Cu-HyS-NaOH are 1.73 and 1.68 eV, respectively. Thus, based on the estimated  $E_g$  of these samples by UV-DRS results, the conduction band (CB) of Cu-HyS-urea and Cu-HyS-NaOH can be calculated to  $-1.9$  and  $-2.15$  eV, respectively.



**Figure 5.** XPS spectra of Cu-HyS-urea and Cu-HyS-NaOH: (a) survey spectra, (b) O 1s, (c) Cu 2p, and (d) valence band energy region.

### 3.2. Hexavalent Chromium (Cr(VI)) Removal

From previous reports, the hydrotalcite-like copper hydroxyl salts (Cu-HyS-urea and Cu-HyS-NaOH) have been utilized as adsorbents and oxidative catalysts for catalytic wet oxidation with and without peroxide [3–5,13]. However, there are no reports about the photocatalytic activity of the hydrotalcite-like copper hydroxyl salts. Thus, the adsorption and photocatalytic activity of Cu-HyS-urea and Cu-HyS-NaOH were examined by conversion of Cr(VI) under dark for adsorption test and light irradiation for photocatalytic reaction test. As shown in Figure 6a, the Cu-HyS-NaOH showed higher adsorption ability of Cr(VI) in the dark condition compared with the Cu-HyS-urea due to the higher SSA of Cu-HyS-NaOH. However, when the reaction was performed under light irradiation, the increase of Cr(VI) reduction activity can be observed for both of Cu-HyS-urea and Cu-HyS-

NaOH samples. The photolysis of Cr(VI) reduction activity during light irradiation was observed less than 0.1% after 60 min under light irradiation. In comparison to the adsorption and photocatalytic reduction after 60 min, as shown in Figure 6b, the Cu-HyS-NaOH presented a total removal efficiency (adsorption and photocatalytic reduction) of about 82%, which was higher than Cu-HyS-urea (36.0%). The main process to remove Cr(VI) using Cu-HyS-NaOH is the adsorption process (53.9%), while the Cu-HyS-urea showed only 0.6% for Cr(VI) adsorption. To compare the photocatalytic reduction activity, it is clear that the Cu-HyS-urea showed a higher photocatalytic reduction of Cr(VI) (35.4%) than Cu-HyS-NaOH (28.1%). The higher photocatalytic activity of Cu-HyS-urea can be explained by its smaller  $E_g$  and high light absorption ability due to  $\text{CO}_3^{2-}$  intercalation. Moreover, the lower  $E_g$  enhances the light absorption of this material, resulting in more production of electrons for the Cr(VI) reduction. To compare with the other, Cu-HyS-urea exhibited excellent Cr(VI) reduction and was comparable with the other composite materials such as  $\text{Fe}_3\text{O}_4$ -ZnAl-layered double hydroxide/ $\text{TiO}_2$  composites [44], acid modified  $\text{g-C}_3\text{N}_4$  [45], MWCNTs- $\text{Fe}_3\text{O}_4$ @PES nanofibers [46], and char/ $\text{TiO}_2$  composite photocatalyst [47], which are difficult to synthesize. Thus, Cu-HyS-urea can be an alternative photocatalyst for practical wastewater management with easy preparation and high Cr(VI) removal efficiency.

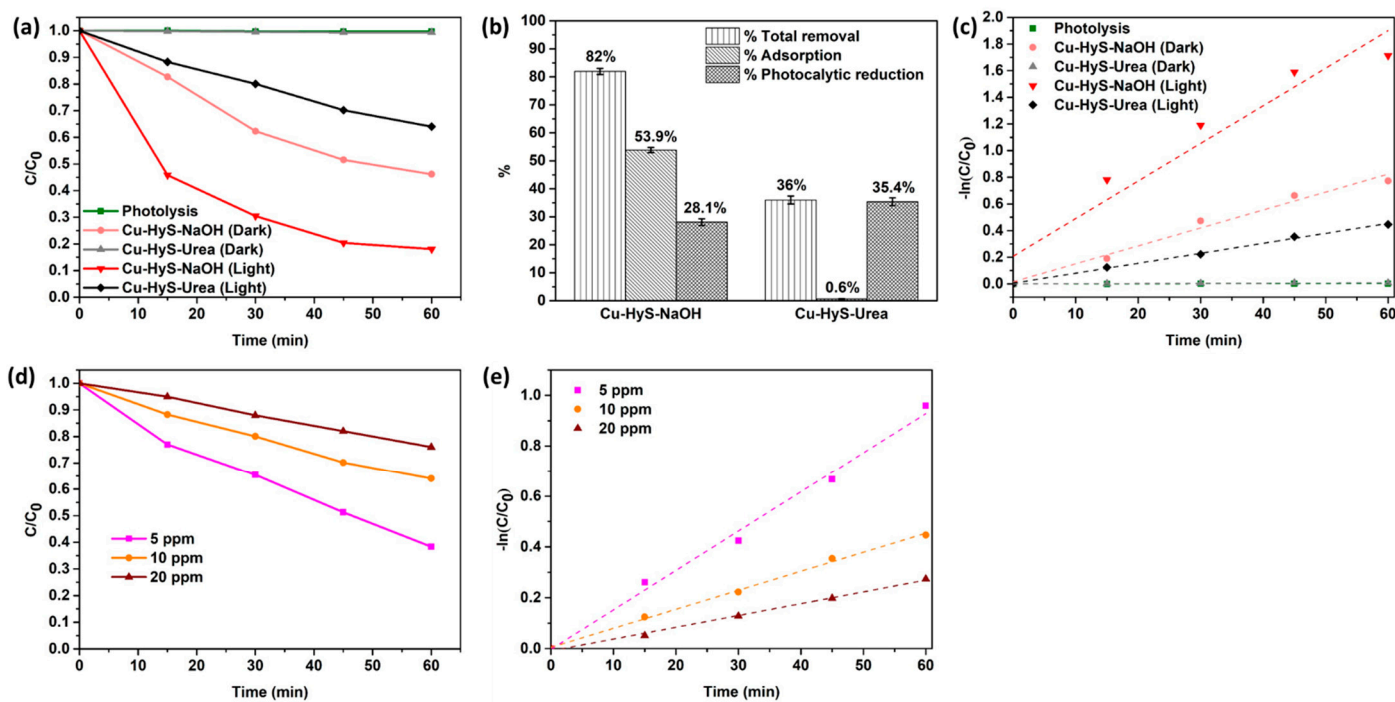


**Figure 6.** (a) Photocatalytic reduction of Cr(VI), (b) removal efficiency over Cu-HyS-urea and Cu-HyS-NaOH, (c) kinetics plots of photocatalytic reduction of Cr(VI), (d) effect of concentration of Cr(VI) for the photocatalytic reduction over Cu-HyS-urea, and (e) kinetics plots of the effect of concentration of Cr(VI).

Moreover, the photocatalytic Cr(VI) removal kinetics of the Cu-HyS-urea and Cu-HyS-NaOH were fitted using the pseudo-first-order kinetic model, which was generally utilized to analyze the kinetics of the photocatalytic degradation [48], as shown in Figure 6c. The reaction rate constants ( $k$ ) of photolysis, Cu-HyS-NaOH (dark), Cu-HyS-urea (dark), Cu-HyS-NaOH (light), and Cu-HyS-urea (light) are  $0.00005 \text{ min}^{-1}$  ( $R^2 = 0.93$ ),  $0.013 \text{ min}^{-1}$  ( $R^2 = 0.93$ ),  $0.00011 \text{ min}^{-1}$  ( $R^2 = 0.92$ ),  $0.028 \text{ min}^{-1}$  ( $R^2 = 0.90$ ), and  $0.007 \text{ min}^{-1}$  ( $R^2 = 0.99$ ), respectively. In comparison, the main process to remove Cr(VI) using Cu-HyS-Urea is photocatalytic reduction. Thus, this is a reason that the Cr(VI) reduction efficiency was well-fitted with the pseudo-first-order kinetic model ( $R^2 = 0.99$ ), which is usually used for

photocatalytic reactions due to it having less adsorption of Cr(VI). However, the low value of  $R^2$  (0.90) of the Cr(VI) removal over Cu-HyS-NaOH with the pseudo-first-order kinetic model may be because the removal of Cr(VI) not only comes from photocatalytic reduction, but also some Cr(VI) can be adsorbed on the surface of Cu-HyS-NaOH via adsorption, which showed the large fraction of adsorption compared with Cu-HyS-urea.

The rate constant of Cu-HyS-NaOH (light) was highest, approximately two and four times higher than that of Cu-HyS-NaOH (dark) and Cu-HyS-urea (light), while the Cu-HyS-urea (light) showed a higher reaction rate constant about 64 times higher than that of Cu-HyS-urea (dark). These results suggest that the Cu-HyS-urea has a higher photocatalytic performance for Cr(VI) reduction than Cu-HyS-NaOH. In addition, the effect of Cr(VI) concentration for photocatalytic Cr(VI) reduction was examined using the Cu-HyS-urea which has less adsorption and high photocatalytic activity, as shown in Figure 6d. It can be seen that the photocatalytic activity decreased when the concentration of Cr(VI) increased. The Cr(VI) reduction performance dropped from around 62.7% (Cr(VI) = 5 ppm) to 36.0% (Cr(VI) = 20 ppm) and 23.5% (Cr(VI) = 20 ppm). Moreover, the photocatalytic Cr(VI) removal kinetics of different Cr(VI) concentrations over Cu-HyS-urea was calculated, as shown in Figure 6e. The reaction rate constants ( $k$ ) of Cr(VI) at 5 ppm, 10 ppm, and 20 ppm are  $0.0155 \text{ min}^{-1}$  ( $R^2 = 0.99$ ),  $0.007 \text{ min}^{-1}$  ( $R^2 = 0.99$ ), and  $0.005 \text{ min}^{-1}$  ( $R^2 = 0.99$ ), respectively. Thus, these results suggest that the Cu-HyS-urea can be used for Cr(VI) reduction at high concentrations, but the reaction speed will be decreased due to high competitive reaction between Cr(VI) and photogenerated electrons from Cu-HyS-urea.

In the reusability test, we would like to emphasize the new function of Cu-HyS as a photocatalyst. Thus, we focused on the Cu-HyS-urea because the Cu-HyS-urea showed the highest photocatalytic Cr(VI) reduction activity. Thus, the stability and reusability of Cu-HyS-urea were evaluated by the XRD investigation of a used Cu-HyS-urea after Cr(VI) reduction and a recyclability test for five cycles of Cr(VI) reduction. It can be seen that the spent XRD pattern of the Cu-HyS-urea did not change after Cr(VI) reduction, confirming that the Cu-HyS-urea has high stability for Cr(VI) reduction (Figure 7a,b). However, the decreasing XRD intensity of the spent catalyst may be caused by some destructuring or adsorption of Cr ions on the surface of the spent catalyst. Moreover, the removal efficiency of Cr(VI) over Cu-HyS-urea was maintained for five cycles with a high Cr(VI) reduction efficiency of approximately 35% after 60 min (Figure 7c), indicating that Cu-HyS-urea has high stability and reusability for Cr(VI) reduction under light illumination. According to the World Health Organization worldwide drinking-water guidelines, Cr(VI) has a maximum permitted content of 0.05 mg/L, while copper is an important nutrient and a drinking-water pollutant with a daily dose of roughly 1 mg [49]. As a result, the utilization of a Cu-HyS catalyst could generate lower harm than the Cr(VI) solution.

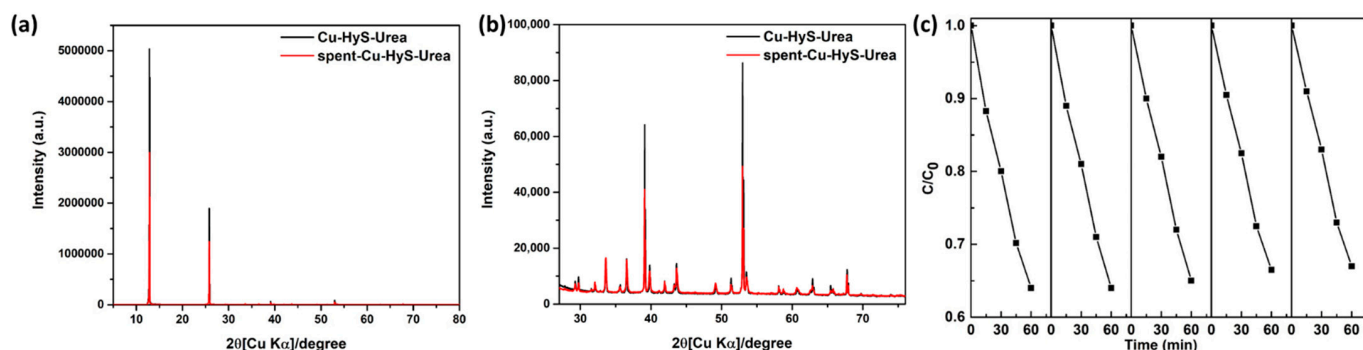


**Figure 7.** XRD patterns of Cu-HyS-urea and spent-Cu-HyS-urea (a) at  $2\theta = 5^\circ\text{--}80^\circ$ , (b)  $2\theta = 27^\circ\text{--}76^\circ$  and (c) reusability of Cr(VI) reduction over Cu-HyS-urea.

### 3.3. Verification of Charge Transfer, Separation and Production of Electron and Hole

The effect of the preparation methods (urea hydrolysis and precipitation) of the hydroxalite-like copper hydroxyl salts (Cu-HyS-urea and Cu-HyS-NaOH) on the electron–

hole recombination and transfer of the electron was investigated using PL, transient photocurrent response measurements, and EIS. Figure 8a illustrates the PL spectra of Cu-HyS-urea and Cu-HyS-NaOH in the emission wavelength range of 400–480 nm with the maximum emission peak at 442 nm (excitation wavelength at 330 nm). A lower PL intensity refers to a lower photogenerated electron–hole pair recombination rate [50,51]. The Cu-HyS-urea sample showed a lower PL emission intensity than Cu-HyS-NaOH at a wavelength of approximately 442 nm for the excitation wavelength at 370 nm, which implies that the high crystallinity of Cu-HyS-urea and some intercalation of carbonate anions in the structure of hydroxalate-like copper hydroxyl salts can enhance the separation of the photogenerated electron–hole pairs in the Cu-HyS-urea. Furthermore, the electron production and electron transfer of Cu-HyS-urea and Cu-HyS-NaOH during light irradiation were also investigated by transient photocurrent responsive performance, and the results are shown in Figure 8b. Indeed, Cu-HyS-urea displays a higher photocurrent density than Cu-HyS-NaOH, suggesting the Cu-HyS-urea, which has a lower  $E_g$ , can produce more electron–hole pairs with highly efficient charge separation under light irradiation. In addition, the electron transfers and separation properties were studied using electrochemical impedance spectroscopy (EIS) measurements. Normally, the smaller radius of the EIS Nyquist diagram implies a lower electron transfer resistance. In Figure 8c, the smallest radius of the EIS Nyquist diagram was obtained in the Cu-HyS-urea compared with that observed for Cu-HyS-NaOH, implying that the Cu-HyS-urea may have better facilitation of electron transfer. Therefore, the results from PL spectroscopy, transient photocurrent density, and EIS measurements confirmed the hydroxalate-like copper hydroxyl salts from urea hydrolysis (Cu-HyS-urea) can provide a higher charge separation and production due to small  $E_g$  and high crystallinity.

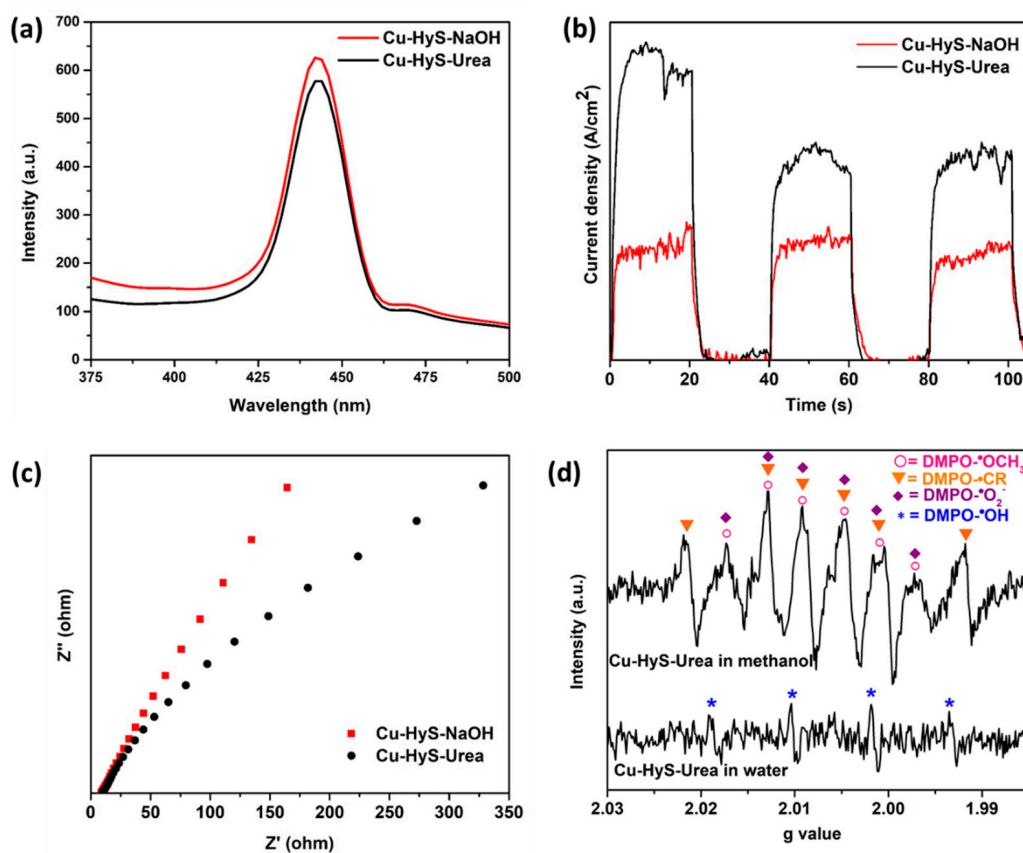


**Figure 8.** Electrochemical characteristics of samples' (a) photoluminescence spectra, (b) photocurrent response, (c) electrochemical impedance spectra, and (d) ESR spectra.

To prove the production of electron–hole pairs, which may further produce some active radicals from the photocatalytic reaction, electron spin resonance (ESR) spectroscopy was utilized. To further observe the reactive radical species, the ESR signal of spin adduct by using DMPO as the spin trapping reagent is shown in Figure 8d. In an aqueous solution, the weak four-line signals of hyperfine splitting pattern giving the intensity peak ratio equal to 1:2:2:1 can be assigned to the DMPO-•OH adduct ( $a_N = 15.0$  G and  $a_H = 14.7$  G;  $g = 2.0059$ ), which confirms the formation of •OH radicals [52,53]. For methanol dispersion, the eight-line signal was identified by the fitting, which revealed 93% simulation correlation with the three main compositions, 56.7% DMPO-•OCH<sub>3</sub> ( $a_N = 13.63$  G,  $a_H^\beta = 7.90$  G,  $a_H^\gamma = 1.67$  G;  $g = 2.0057$ ), 37.9% DMPO-•CR ( $a_N = 14.8$ ,  $a_H^\beta = 22.0$  G;  $g = 2.0057$ ), and 5.4% DMPO-•O<sub>2</sub><sup>-</sup> ( $a_N = 13.76$ ,  $a_H^\beta = 9.63$ ,  $a_H^\gamma = 1.36$  G;  $g = 2.0057$ ) [52]. The appearance of DMPO-•OCH<sub>3</sub> confirmed the generation of h<sup>+</sup> in the VB that was further reacted with the methanol to produce •OCH<sub>3</sub> radicals, while the formation of •O<sub>2</sub><sup>-</sup> radicals implies the generation of photogenerated electrons, which react with dissolved O<sub>2</sub> in the media to produce •O<sub>2</sub><sup>-</sup> radicals. Thus, these results suggest that the hydrotalcite-like copper hydroxyl salts (Cu-HyS-urea and Cu-HyS-NaOH) can act as a photocatalyst for Cr(VI) reduction.

### 3.4. Photocatalytic Mechanism

Based on the above results, the proposed mechanism for photocatalytic reduction of Cr(VI) over the hydrotalcite-like copper hydroxyl salts (Cu-HyS-urea and Cu-HyS-NaOH) is shown in Figure 9. From the electronic position results, the VB of Cu-HyS-urea was 1.73 eV, which was higher than the VB of Cu-HyS-NaOH at 1.68 eV, while the CB of Cu-HyS-urea at -1.9 eV was more positive than that of CN at -2.15 eV. Thus, under light irradiation, both the Cu-HyS-urea and Cu-HyS-NaOH photocatalysts, which have  $E_g$  values of approximately 2.95 eV and 3.39 eV, respectively, can excite electrons from VB to CB, simultaneously generating holes in the VB. For the photocatalytic conversion of Cr(VI), the accumulated electrons in the CB of both hydrotalcite-like copper hydroxyl salts can react with Cr(VI)O<sub>4</sub><sup>2-</sup> in the solution to reduce them to Cr(III). Simultaneously, holes (h<sup>+</sup>) in the VB of both hydrotalcite-like copper hydroxyl salts were consumed by their reaction with the ethanol, which acts as a hole scavenger to remove the hole in the VB to prevent the re-oxidation of reduced Cr(III). Thus, the hydrotalcite-like copper hydroxyl salts (Cu-HyS-urea and Cu-HyS-NaOH) can be used not only as an adsorbent for adsorption of Cr(VI) but also act as a photocatalyst to reduce Cr(VI) to Cr(III), which has less toxicity.

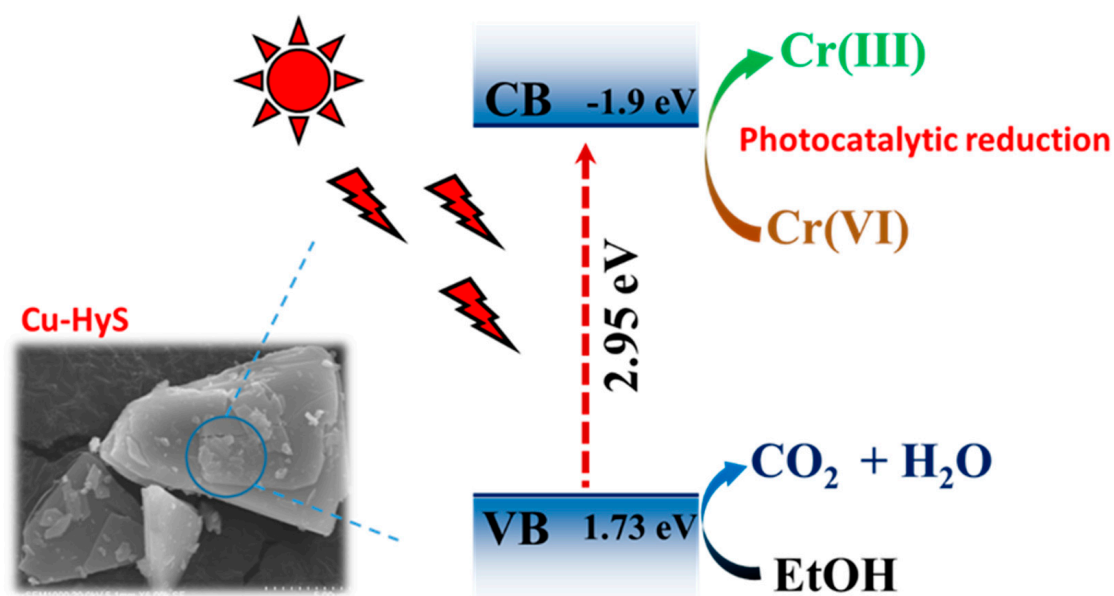


Figure 9. Proposed photocatalytic Cr(VI) reduction over Cu-HyS-urea.

#### 4. Conclusions

Hydrotalcite-like copper hydroxyl salts (Cu-HyS-urea and Cu-HyS-NaOH) were successfully synthesized by two different methods, which were urea hydrolysis and precipitation, and they were applied for the removal of 10 ppm Cr, which is a toxic inorganic pollutant in wastewater. The obtained products from urea hydrolysis (Cu-HyS-urea) showed higher crystallinity, better light absorption ability, and smaller  $E_g$  than the Cu-HyS-NaOH, which was prepared from precipitation. The improvement of crystallinity and optical properties of the Cu-HyS-urea may have resulted from the intercalation of carbonate anions generated from the decomposition of urea during the formation of hydrotalcite-like copper hydroxyl salts from urea hydrolysis. For the 10 ppm Cr(VI) removal, the Cu-HyS-NaOH showed higher Cr(VI) adsorption ability than Cu-HyS-urea because the Cu-HyS-NaOH has higher SSA, confirmed by BET analysis. However, the highest photocatalytic 10 ppm Cr(VI) reduction activity was obtained for Cu-HyS-urea, which showed around 35.4%, while the Cu-HyS-NaOH presented a photocatalytic Cr(VI) reduction of about 28%. The best photocatalytic performance for the photocatalytic reduction of 10 ppm Cr(VI) was compared by using Cu-HyS-urea and can be explained by its smaller  $E_g$  due to the intercalation of carbonate anions. Moreover, the PL, photocurrent response, EIS, and ERDT results suggested that the high crystallinity of Cu-HyS-urea can promote the separation of electron–hole pairs and transfer of the charge carriers, resulting in enhanced photocatalytic activity for Cr(VI) reduction. Thus, these results suggest that the formation of hydrotalcite-like copper hydroxyl salts by urea hydrolysis can develop photocatalytic activity by improvement of its optical properties. This work proves that the hydrotalcite-like copper hydroxyl salts (Cu-HyS-urea and Cu-HyS-NaOH) can be utilized not only as an adsorbent, but they can also act as a photocatalyst to reduce the toxicity of Cr(VI) in wastewater under light irradiation.

**Supplementary Materials:** The following supporting information can be downloaded at: <https://www.mdpi.com/article/10.3390/min12020182/s1>, Figure S1: Spectral radiance of the 500 W Xe lamp.

**Author Contributions:** Conceptualization, C.C. and K.S. (Keiko Sasaki); investigation, C.C., S.M.S. and K.S. (Keiko Sasaki); formal analysis, C.C., K.S. (Karthikeyan Sekar), V.B., L.Z. and J.T.; writing original draft, C.C.; writing—review and editing, C.C. and K.S. (Keiko Sasaki); project administration and funding acquisition, K.S. (Keiko Sasaki). All authors have read and agreed to the published version of the manuscript.

**Funding:** This research was funded by the Japan Society for the Promotion of Science (JSPS) KAKENHI (A), grant no. JP19F19393, and Kyushu University (Progress 100).

**Acknowledgments:** ESR measurements were supported by the Center of Excellence for Innovation in Chemistry (PERCH-CIC), Ministry of Higher Education, Science, Research and Innovation.

**Conflicts of Interest:** The authors declare no conflict of interest.

#### References

1. Thomas, N. Mechanochemical synthesis of layered hydroxy salts. *Mater. Res. Bull.* **2012**, *47*, 3568–3572. [[CrossRef](#)]
2. Li, B.-C.; Huy, N.N.; Lin, J.-Y.; Phattarapattamawong, S.; Lisak, G.; Wang, H.; Lin, K.-Y.A. Nanopetal-like copper hydroxide nitrate as a highly selective heterogeneous catalyst for valorization of vanillic alcohol via oxidation. *J. Environ. Chem. Eng.* **2021**, *9*, 106092. [[CrossRef](#)]
3. Srikaow, A.; Smith, S.M.; Uraisin, K.; Suttiponparnit, K.; Kongmark, C.; Chuaicham, C. Catalytic remediation of phenol contaminated wastewater using Cu–Zn hydroxide nitrate. *RSC Adv.* **2016**, *6*, 36766–36774. [[CrossRef](#)]
4. Weeramankhontert, V.; Srikaow, A.; Smith, S.M. Formation of copper hydroxy double salts derived from metal oxides and their catalytic activity in degradation of methyl orange. *Ceram. Int.* **2019**, *45*, 993–1000. [[CrossRef](#)]
5. Wang, S.; Zhang, X.; Pan, L.; Zhao, F.-M.; Zou, J.-J.; Zhang, T.; Wang, L. Controllable sonochemical synthesis of  $\text{Cu}_2\text{O}/\text{Cu}_2(\text{OH})_3\text{NO}_3$  composites toward synergy of adsorption and photocatalysis. *Appl. Catal. B Environ.* **2015**, *164*, 234–240. [[CrossRef](#)]
6. Anandan, S.; Wu, J.J.; Ashokkumar, M. Sonochemical Synthesis of Layered Copper Hydroxy Nitrate Nanosheets. *ChemPhysChem* **2015**, *16*, 3389–3391. [[CrossRef](#)]

7. da Rocha, M.G.; Nakagaki, S.; Ucoski, G.M.; Wypych, F.; Sippel Machado, G. Comparison between catalytic activities of two zinc layered hydroxide salts in brilliant green organic dye bleaching. *J. Colloid Interface Sci.* **2019**, *541*, 425–433. [[CrossRef](#)]
8. Dai, T.; Mao, Y. ZnO-assisted synthesis of multilayered Cu<sub>2</sub>(OH)<sub>3</sub>NO<sub>3</sub> nanoplates and application removal of methyl orange. *Chem. Phys. Lett.* **2020**, *739*, 137018. [[CrossRef](#)]
9. Gao, J.; Yuan, X. Vibrational Investigation of Pressure-Induced Phase Transitions of Hydroxycarbonate Malachite Cu<sub>2</sub>(CO<sub>3</sub>)(OH)<sub>2</sub>. *Minerals* **2020**, *10*, 277. [[CrossRef](#)]
10. Henrist, C.; Traina, K.; Hubert, C.; Toussaint, G.; Rulmont, A.; Cloots, R. Study of the morphology of copper hydroxynitrate nanoplatelets obtained by controlled double jet precipitation and urea hydrolysis. *J. Cryst. Growth* **2003**, *254*, 176–187. [[CrossRef](#)]
11. Liu, B. One-dimensional copper hydroxide nitrate nanorods and nanobelts for radiochemical applications. *Nanoscale* **2012**, *4*, 7194–7198. [[CrossRef](#)] [[PubMed](#)]
12. Yu, Q.; Huang, H.; Chen, R.; Wang, P.; Yang, H.; Gao, M.; Peng, X.; Ye, Z. Synthesis of CuO nanowalnuts and nanoribbons from aqueous solution and their catalytic and electrochemical properties. *Nanoscale* **2012**, *4*, 2613–2620. [[CrossRef](#)] [[PubMed](#)]
13. Sriksaow, A.; Smith, S.M. Preparation of Cu<sub>2</sub>(OH)<sub>3</sub>NO<sub>3</sub>/ZnO, a novel catalyst for methyl orange oxidation under ambient conditions. *Appl. Catal. B Environ.* **2013**, *130–131*, 84–92. [[CrossRef](#)]
14. Videira-Quintela, D.; Guillén, F.; Montalvo, G.; Martin, O. Silver, copper, and copper hydroxy salt decorated fumed silica hybrid composites as antibacterial agents. *Colloids Surf. B Biointerfaces* **2020**, *195*, 111216. [[CrossRef](#)] [[PubMed](#)]
15. Balakumar, V.; Manivannan, R.; Chuaicham, C.; Karthikeyan, S.; Sasaki, K. A simple tactic synthesis of hollow porous graphitic carbon nitride with significantly enhanced photocatalytic performance. *Chem. Commun.* **2021**, *57*, 6772–6775. [[CrossRef](#)] [[PubMed](#)]
16. Balakumar, V.; Ramalingam, M.; Sekar, K.; Chuaicham, C.; Sasaki, K. Fabrication and characterization of carbon quantum dots decorated hollow porous graphitic carbon nitride through polyaniline for photocatalysis. *Chem. Eng. J.* **2021**, *426*, 131739. [[CrossRef](#)]
17. Chuaicham, C.; Inoue, T.; Balakumar, V.; Tian, Q.; Ohtani, B.; Sasaki, K. Visible light-driven ZnCr double layer oxide photocatalyst composites with fly ashes for the degradation of ciprofloxacin. *J. Environ. Chem. Eng.* **2021**, *10*, 106970. [[CrossRef](#)]
18. Chuaicham, C.; Sekar, K.; Xiong, Y.; Balakumar, V.; Mittraphab, Y.; Shimizu, K.; Ohtani, B.; Dabo, I.; Sasaki, K. Single-step synthesis of oxygen-doped hollow porous graphitic carbon nitride for photocatalytic ciprofloxacin decomposition. *Chem. Eng. J.* **2021**, *425*, 130502. [[CrossRef](#)]
19. Chuaicham, C.; Xiong, Y.; Sekar, K.; Chen, W.; Zhang, L.; Ohtani, B.; Dabo, I.; Sasaki, K. A promising Zn-Ti layered double hydroxide/Fe-bearing montmorillonite composite as an efficient photocatalyst for Cr(VI) reduction: Insight into the role of Fe impurity in montmorillonite. *Appl. Surf. Sci.* **2021**, *546*, 148835. [[CrossRef](#)]
20. Sekar, K.; Chuaicham, C.; Vellaichamy, B.; Li, W.; Zhuang, W.; Lu, X.; Ohtani, B.; Sasaki, K. Cubic Cu<sub>2</sub>O nanoparticles decorated on TiO<sub>2</sub> nanofiber heterostructure as an excellent synergistic photocatalyst for H<sub>2</sub> production and sulfamethoxazole degradation. *Appl. Catal. B Environ.* **2021**, *294*, 120221. [[CrossRef](#)]
21. Pereira Rocha, R.L.; Silva, T.L.; Araujo, F.P.; Vieira, E.G.; Honório, L.M.; Furtini, M.B.; da Fonseca, M.G.; Silva-Filho, E.C.d.; Osajima, J.A. Gallium-Containing Hydroxyapatite as a Promising Material for Photocatalytic Performance. *Minerals* **2021**, *11*, 1347. [[CrossRef](#)]
22. Bouddouch, A.; Amaterz, E.; Bakiz, B.; Taoufyq, A.; Guinneton, F.; Villain, S.; Gavarrì, J.-R.; Valmalette, J.-C.; Benlhachemi, A. Phase Transformation, Photocatalytic and Photoluminescent Properties of BiPO<sub>4</sub> Catalysts Prepared by Solid-State Reaction: Degradation of Rhodamine B. *Minerals* **2021**, *11*, 1007. [[CrossRef](#)]
23. Zhang, L.; Chuaicham, C.; Balakumar, V.; Ohtani, B.; Sasaki, K. Fabrication of Adsorbed Fe(III) and Structurally Doped Fe(III) in Montmorillonite/TiO<sub>2</sub> Composite for Photocatalytic Degradation of Phenol. *Minerals* **2021**, *11*, 1381. [[CrossRef](#)]
24. Shabalala, A.N.; Basitere, M. Interactive Relationship between Cementitious Materials and Acid Mine Drainage: Their Effects on Chromium Cr(VI) Removal. *Minerals* **2020**, *10*, 932. [[CrossRef](#)]
25. Chen, C.; Zeng, H.; Xiong, J.; Xu, S.; An, D. Z-scheme AgBr@Ag/CoAl layered double hydroxide heterojunction for superior photocatalytic Cr(VI) reduction under visible light. *Appl. Clay Sci.* **2020**, *192*, 105627. [[CrossRef](#)]
26. Cheng, C.; Chen, D.; Li, N.; Li, H.; Xu, Q.; He, J.; Lu, J. Construction of hollow In<sub>2</sub>S<sub>3</sub>/CdIn<sub>2</sub>S<sub>4</sub> heterostructures with high efficiency for Cr(vi) reduction. *Environ. Sci. Nano* **2021**, *8*, 1389–1397. [[CrossRef](#)]
27. Padhi, D.K.; Panigrahi, T.K.; Parida, K.; Singh, S.K.; Mishra, P.M. Green Synthesis of Fe<sub>3</sub>O<sub>4</sub>/RGO Nanocomposite with Enhanced Photocatalytic Performance for Cr(VI) Reduction, Phenol Degradation, and Antibacterial Activity. *ACS Sustain. Chem. Eng.* **2017**, *5*, 10551–10562. [[CrossRef](#)]
28. Yuan, X.Y.; Jing, Q.Y.; Chen, J.T.; Li, L. Photocatalytic Cr(VI) reduction by mixed metal oxide derived from ZnAl layered double hydroxide. *Appl. Clay Sci.* **2017**, *143*, 168–174. [[CrossRef](#)]
29. Yuan, G.; Li, F.; Li, K.; Liu, J.; Li, J.; Zhang, S.; Jia, Q.; Zhang, H. Research Progress on Photocatalytic Reduction of Cr(VI) in Polluted Water. *Bull. Chem. Soc. Jpn.* **2020**, *94*, 1142–1155. [[CrossRef](#)]
30. El-Taweel, Y.A.; Nassef, E.M.; Elkheriany, I.; Sayed, D. Removal of Cr(VI) ions from waste water by electrocoagulation using iron electrode. *Egypt. J. Pet.* **2015**, *24*, 183–192. [[CrossRef](#)]
31. Zhang, S.; Zhang, H.; Liu, F.; Yang, F.; Zhou, S.; Zheng, K.; Chu, C.; Liu, L.; Ju, M. Effective removal of Cr(vi) from aqueous solution by biochar supported manganese sulfide. *RSC Adv.* **2019**, *9*, 31333–31342. [[CrossRef](#)]
32. Valizadeh, B.; Nguyen, T.N.; Kampouri, S.; Sun, D.T.; Mensi, M.D.; Stylianou, K.; Smit, B.; Queen, W.L. A novel integrated Cr(vi) adsorption–photoreduction system using MOF@polymer composite beads. *J. Mater. Chem. A* **2020**, *8*, 9629–9637. [[CrossRef](#)]

33. Rahmani, A.r.; Hossieni, E.; Poormohammadi, A. Removal of Chromium (VI) from Aqueous Solution Using Electro-Fenton Process. *Environ. Processes* **2015**, *2*, 419–428. [[CrossRef](#)]
34. Higgins, T.E.; Halloran, A.R.; Petura, J.C. Traditional and innovative treatment methods for Cr(VI) in soil. *J. Soil Contam.* **1997**, *6*, 767–797. [[CrossRef](#)]
35. Chuaicham, C.; Karthikeyan, S.; Pawar, R.R.; Xiong, Y.; Dabo, I.; Ohtani, B.; Kim, Y.; Song, J.T.; Ishihara, T.; Sasaki, K. Energy-resolved distribution of electron traps for O/S-doped carbon nitrides by reversed double-beam photoacoustic spectroscopy and the photocatalytic reduction of Cr(vi). *Chem. Commun.* **2020**, *56*, 3793–3796. [[CrossRef](#)] [[PubMed](#)]
36. Zhan, Y.; Zhou, X.; Fu, B.; Chen, Y. Catalytic wet peroxide oxidation of azo dye (Direct Blue 15) using solvothermally synthesized copper hydroxide nitrate as catalyst. *J. Hazard. Mater.* **2011**, *187*, 348–354. [[CrossRef](#)]
37. Jia, J.; Wang, H.; Niu, H.; Chen, J.; Song, J.; Mao, C.; Zhang, S.; Gao, Y.; Chen, C. Highly selective adsorption of organic dyes containing sulphonic groups using  $\text{Cu}_2(\text{OH})_3\text{NO}_3$  nanosheets. *J. Nanopart. Res.* **2016**, *18*, 260. [[CrossRef](#)]
38. Parida, K.M.; Mohapatra, L. Carbonate intercalated Zn/Fe layered double hydroxide: A novel photocatalyst for the enhanced photo degradation of azo dyes. *Chem. Eng. J.* **2012**, *179*, 131–139. [[CrossRef](#)]
39. Rajamathi, J.T.; Britto, S.; Rajamathi, M. Synthesis and anion exchange reactions of a layered copper-zinc hydroxy double salt,  $\text{Cu}_{1.6}\text{Zn}_{0.4}(\text{OH})_3(\text{OAc})\cdot\text{H}_2\text{O}$ . *J. Chem. Sci.* **2005**, *117*, 629–633. [[CrossRef](#)]
40. Sun, S.; Zhang, X.; Sun, Y.; Yang, S.; Song, X.; Yang, Z. Hierarchical CuO nanoflowers: Water-required synthesis and their application in a nonenzymatic glucose biosensor. *Phys. Chem. Chem. Phys.* **2013**, *15*, 10904–10913. [[CrossRef](#)]
41. Bourenane, N.; Hamlaoui, Y.; Remazeilles, C.; Pedraza, F. Effect of the pH of the electrolyte on the formation and on the corrosion properties of ceria based coating on carbon steel. *Mater. Corros.* **2019**, *70*, 110–119. [[CrossRef](#)]
42. Wang, C.; Higgins, D.; Wang, F.; Li, D.; Liu, R.; Xia, G.; Li, N.; Li, Q.; Xu, H.; Wu, G. Controlled synthesis of micro/nanostructured CuO anodes for lithium-ion batteries. *Nano Energy* **2014**, *9*, 334–344. [[CrossRef](#)]
43. Liang, W.; Zhu, L.; Li, W.; Liu, H. Facile fabrication of a flower-like  $\text{CuO}/\text{Cu}(\text{OH})_2$  nanorod film with tunable wetting transition and excellent stability. *RSC Adv.* **2015**, *5*, 38100–38110. [[CrossRef](#)]
44. Yang, Y.; Li, J.; Yan, T.; Zhu, R.; Yan, L.; Pei, Z. Adsorption and photocatalytic reduction of aqueous Cr(VI) by  $\text{Fe}_3\text{O}_4$ -ZnAl-layered double hydroxide/ $\text{TiO}_2$  composites. *J. Colloid Interface Sci.* **2020**, *562*, 493–501. [[CrossRef](#)] [[PubMed](#)]
45. Wei, H.; Zhang, Q.; Zhang, Y.; Yang, Z.; Zhu, A.; Dionysiou, D.D. Enhancement of the Cr(VI) adsorption and photocatalytic reduction activity of g-C<sub>3</sub>N<sub>4</sub> by hydrothermal treatment in  $\text{HNO}_3$  aqueous solution. *Appl. Catal. A Gen.* **2016**, *521*, 9–18. [[CrossRef](#)]
46. Mohamed, A.; Yousef, S.; Ali, S.; Sriubas, M.; Varnagiris, S.; Tuckute, S.; Abdelnaby, M.A.; Kamel, B.M. Highly Efficient Visible Light Photodegradation of Cr(VI) Using Electrospun MWCNTs- $\text{Fe}_3\text{O}_4$ @PES Nanofibers. *Catalysts* **2021**, *11*, 868. [[CrossRef](#)]
47. Antonopoulou, M.; Chondrodinou, I.; Bairamis, F.; Giannakas, A.; Konstantinou, I. Photocatalytic reduction of Cr(VI) by char/ $\text{TiO}_2$  composite photocatalyst: Optimization and modeling using the response surface methodology (RSM). *Environ. Sci. Pollut. Res.* **2017**, *24*, 1063–1072. [[CrossRef](#)]
48. Laipan, M.; Zhu, R.; Zhu, J.; He, H. Visible light assisted Fenton-like degradation of Orange II on  $\text{Ni}_3\text{Fe}/\text{Fe}_3\text{O}_4$  magnetic catalyst prepared from spent FeNi layered double hydroxide. *J. Mol. Catal. A Chem.* **2016**, *415*, 9–16. [[CrossRef](#)]
49. Costa, M. Toxicity and Carcinogenicity of Cr(VI) in Animal Models and Humans. *Crit. Rev. Toxicol.* **1997**, *27*, 431–442. [[CrossRef](#)] [[PubMed](#)]
50. Karthikeyan, S.; Chuaicham, C.; Pawar, R.R.; Sasaki, K.; Li, W.; Lee, A.F.; Wilson, K. Template free mild hydrothermal synthesis of core-shell  $\text{Cu}_2\text{O}(\text{Cu})@\text{CuO}$  visible light photocatalysts for N-acetyl-para-aminophenol degradation. *J. Mater. Chem. A* **2019**, *7*, 20767–20777. [[CrossRef](#)]
51. Sekar, K.; Chuaicham, C.; Balijapalli, U.; Li, W.; Wilson, K.F.; Lee, A.; Sasaki, K. Surfactant- and template-free hydrothermal assembly of  $\text{Cu}_2\text{O}$  visible light photocatalysts for trimethoprim degradation. *Appl. Catal. B Environ.* **2021**, *284*, 119741. [[CrossRef](#)]
52. Dvoranova, D.; Barbierikova, Z.; Brezova, V. Radical intermediates in photoinduced reactions on  $\text{TiO}_2$  (an EPR spin trapping study). *Molecules* **2014**, *19*, 17279–17304. [[CrossRef](#)] [[PubMed](#)]
53. Hou, L.; Li, X.; Yang, Q.; Chen, F.; Wang, S.; Ma, Y.; Wu, Y.; Zhu, X.; Huang, X.; Wang, D. Heterogeneous activation of peroxymonosulfate using Mn-Fe layered double hydroxide: Performance and mechanism for organic pollutant degradation. *Sci. Total Environ.* **2019**, *663*, 453–464. [[CrossRef](#)] [[PubMed](#)]